Connections between Potential Vorticity Intrusions and Convection in the Eastern Tropical Pacific

BEATRIZ M. FUNATSU* AND DARRYN W. WAUGH

Department of Earth and Planetary Science, Johns Hopkins University, Baltimore, Maryland

(Manuscript received 18 July 2006, in final form 16 May 2007)

ABSTRACT

The connections between intrusions of stratospheric air into the upper troposphere and deep convection in the tropical eastern Pacific are examined using a combination of data analysis, potential vorticity (PV) inversion, and numerical simulations. Analysis of NCEP–NCAR reanalyses and satellite measurements of outgoing longwave radiation during intrusion events shows increased cloudiness, lower static stability, upward motion, and a buildup of convective available potential energy (CAPE) at the leading edge of the intruding tongue of high PV. Potential inversion inversion calculations show that the upper-level PV makes the dominant contribution to the changes in the quantities that characterize convection. This supports the hypothesis that upper-level PV anomalies initiate and support convection by destabilizing the lower troposphere and causing upward motion ahead on the PV tongue. The dominant role of the upper-level PV is confirmed by simulations using the fifth-generation Pennsylvania State University–NCAR Mesoscale Model (MM5). Convection only occurs when the upper-level PV anomaly is present in the simulations, and the relative contribution of the upper-level PV to changes in the quantities that characterize convection is similar to that inferred from the PV inversion calculations.

1. Introduction

Deep convection is a key aspect of the tropical atmosphere. Latent heat release in deep convective regions in the tropics is a very important source of energy for the general circulation of the atmosphere (Hoerling 1992). Also, waves generated from extensive areas of convection can travel around the globe, causing changes in weather away from the source region. Locally, deep convection may be important in cross-tropopause mass exchange (e.g., Lamarque and Hess 1994), and in redistributing water vapor, ozone, and other atmospheric constituents (e.g., Waugh 2005 and references therein).

Local factors, such as temperature, humidity, and wind profiles, exert primary control on the existence and strength of deep convection. Those factors are, in turn, modified by large-scale processes, such as large-scale low-level convergence, or destabilization through quasigeostrophic motion. In the midlatitudes, quasigeostrophic motion often causes environmental destabilization, which favors the occurrence of deep convection. Over the warm oceans in the deep tropics, convection is often controlled by changes in heat and moisture surface fluxes in the boundary layer, which in turn act to decrease the convective inhibition. This was found to be particularly true of the tropical eastern Pacific (Raymond et al. 2003). In the subtropics, the picture is more blurred, with both midlatitude and tropical effects playing a role.

An example of a region where tropical convection may be affected by both midlatitude and tropical effects is the eastern tropical Pacific. During boreal winter there are upper-tropospheric equatorial westerlies in this region, while easterlies prevail at low levels. Several studies have shown that wavelike disturbances with periods between 6 and 30 days propagate from the extratropics into the tropics through this upper-level "westerly duct" (Kiladis and Weickmann 1992a,b; Tomas and Webster 1994; Kiladis 1998). The path, velocity, and energy dispersion of these waves agree well

* Current affiliation: Laboratoire de Meteorologie Dynamique (CNRS)/Palaiseau, Ecole Polytechnique, Palaiseau CEDEX, France.

Corresponding author address: Beatriz Funatsu, Laboratoire de Meteorologie Dynamique (CNRS)/Palaiseau, Ecole Polytechnique, 91128 Palaiseau CEDEX, France.
E-mail: funatsu@lmd.polytechnique.fr

DOI: 10.1175/2007JAS2248.1

with those predicted by the linear theory for Rossby wave propagation (Webster and Holton 1982; Hoskins and Ambrizzi 1993), and they have a significant contribution to the momentum balance in the tropical eastern Pacific region (Kiladis and Feldstein 1994; Kiladis 1998), acting to slow the equatorial westerlies (Kiladis 1998). Moreover, circulation anomalies associated with these disturbances correlate well with outgoing longwave radiation (OLR) anomalies in the central and eastern Pacific (Kiladis and Weickmann 1992b; Kiladis 1998).

The Rossby waves that propagate into the westerly duct region are often of a sufficiently large amplitude that "wave breaking" occurs, producing intrusions of stratospheric air with high potential vorticity (PV) into the tropical upper troposphere (e.g., Waugh and Polvani 2000). Waugh and Funatsu (2003) showed a close link between these PV intrusions and deep convection. Deep convection (low OLR) nearly always occurs at the downstream side of the intrusions identified by Waugh and Polvani (2000). Furthermore, PV intrusions nearly always precede occurrences of deep convection in the tropical eastern Pacific. These PV intrusions have been shown to have a large impact on the distribution of trace constituents in the subtropical upper troposphere (e.g., Scott et al. 2001; Waugh and Funatsu 2003; Waugh 2005; Cooper et al. 2005).

The existing hypothesis for this connection between PV intrusions and convection proposes that the convection occurs as a result of decreased static stability and enhanced upward motion in the area of positive vorticity advection ahead of the intrusive trough (Kiladis and Weickmann 1992b; Kiladis 1998). Hoskins et al. (1985) and Thorpe (1985) showed that a positive (cyclonic) upper-level PV has a less stable potential temperature distribution within and immediately below the anomaly. This decrease in the static stability, together with the translational motion of the anomaly itself, results in a vertical motion in low levels. Physically, the vertical velocity can be understood as a sum of the following two effects (Hoskins et al. 2003; Dixon et al. 2003): isentropic displacement, which is a contribution proportional to the local tendency of buoyancy, and isentropic upglide, which is the contribution of the "advection" of buoyancy. The first effect causes the particle to move either up or down as the isentropes "bend" according to the upper-level anomaly; the second effect causes a parcel of air ahead of the upper-level cyclonic anomaly to move northward and westward with a net upward motion (Dixon et al. 2003). The combined effect is illustrated in Fig. 1.

The above studies have shown a strong relationship between Rossby wave activity propagating into the tropical Pacific and deep convection, and have presented examples where the convection occurs ahead of an intruding tongue of high PV. However, it is not known whether the above hypothesis is correct, or what the exact causal link is between PV intrusions and deep convection.

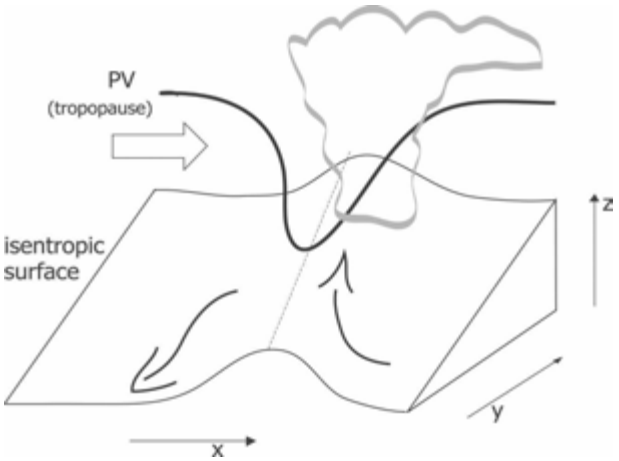

FIG. 1. Schematic representation of the proposed mechanism for the occurrence of convection, based on Dixon et al. (2003). The presence of an upper-level PV trough causes a parcel of air on an isentropic surface to move northwestward and upward on its downstream side, providing conditions favorable to trigger convection.

We address the above issues by examining in detail an intrusion event that occurred between 13 and 17 January 1987, which was previously studied by Kiladis and Weickmann (1992b) and Waugh and Funatsu (2003). Our analysis extends these studies, and involves analysis of both meteorological data and numerical simulations. We first examine the meteorological data to test the hypothesis proposed for the occurrence of convection in the eastern tropical Pacific (section 2), and then to establish a link between intrusions and convection using PV invertibility concepts (section 3). The link between the intrusions and convection is further examined by performing mesoscale model simulations of the event (section 4). Similar analysis of several other intrusion events is also discussed in section 5. A summary and discussion of our findings are presented in section 6.

2. Qualitative analysis

As a first step we investigate whether the data for the intrusion event of 13–17 January 1987 are qualitatively consistent with the proposed theory described above (and illustrated in Fig. 1).

For this analysis we use the 6-hourly National Centers for Environmental Prediction–National Center for

Atmospheric Research (NCEP–NCAR) reanalysis dataset (Kalnay et al. 1996) and daily mean OLR data from the Climate Diagnostic Center (Liebmann and Smith 1996). Both have a horizontal resolution of 2.5° latitude × 2.5° longitude. From the reanalysis data we calculate the potential vorticity

$$\mathrm{PV} = \boldsymbol{\zeta}_a \cdot \frac{\boldsymbol{\nabla}\theta}{\rho}, \tag{1}$$

(where $\boldsymbol{\zeta}_a$ is the three-dimensional absolute vorticity field, θ is the potential temperature, and ρ is the density), the static stability $\mathcal{S} = -g\partial\theta/\partial p$, and the convective available potential energy

$$\mathrm{CAPE} = \int_{\mathrm{LFC}}^{\mathrm{LNB}} g \frac{[\theta_{vp}(z) - \theta_v(z)]}{\theta_v(z)}\, dz \tag{2}$$

[where the integration limits are the level of free convection (LFC) and level of neutral buoyancy (LNB), $\theta_{vp}(z)$ is the virtual potential temperature of the air parcel, and $\theta_v(z)$ is the virtual potential temperature of the environment]. PV is used to identify the intrusions, while OLR, vertical velocity ω, $\mathcal{S}$, and CAPE are used to examine the convective conditions.

The evolution of PV, OLR, and ω for the above data and period is shown in Fig. 2. The contours of PV = 2 PV units (PVU; 1 PVU = 10^{-6} K m^2 kg^{-1} s^{-1}) indicate the position of the dynamical tropopause, which undulates and amplifies in the early stages, turning into a sharp trough by 15 January, and decaying as it moves eastward. On 15 January, an area of low OLR and strong upward motion is observed ahead of the intruding PV trough (see also Kiladis and Weickmann 1992b).

Figure 3a shows latitudinal cross sections at 25°N and Fig. 3b shows longitudinal cross sections at 215°E, which cut through the leading edge of the intrusive tongue of θ, ω, and PV on 15 January 1987. There is decreased static stability downstream of the intrusion at low levels between 1000 and 600 hPa, and 205°–220°E (Fig. 3a). The tilt of the isentropic surface and translation of the system to the east indicate that in a frame of reference moving with the intrusion a particle will move upward and westward in the region downstream of the upper-level trough. Also, Fig. 3b shows that the isentropes slope upward toward the North Pole "ahead" of the intrusion, and therefore in a 3D perspective the particle is moving westward and northward, with a net upward motion in the region ahead of the intrusion. This observation is consistent with the reanalysis ω field (see also Figs. 2 and 4a).

Analysis of daily maps of dry static stability and CAPE shows substantial changes as the intrusion evolves. For example, the solid curves in Fig. 5 show the evolution of $\mathcal{S}$ (Fig. 5a) and CAPE (Fig. 5b) at a grid point located within the area of ascent ahead of the intrusion on 15 January. Consistent with the above arguments, there is a decrease in static stability and increase in CAPE in the 36 h before convection occurred.

The analysis above shows that there is good *qualitative* agreement between the data and the proposed theory, for example, compared with Fig. 1. We next examine the quantitative importance of intrusions to changes in the dynamical and thermodynamical fields.

3. PV inversion

In the previous section we showed that there is decreased static stability and upward vertical motion in an extensive area ahead of the intrusion, and that there is an increase of CAPE as the intrusion evolves and the high-PV ridge amplifies. This is consistent with the hypothesis of Kiladis and Weickmann (1992b) and Kiladis (1998); however, it does not establish a formal link between the PV intrusion and convection. Therefore, in this section we aim at quantifying the changes in θ, ω, and CAPE that are attributable to the upper-level PV anomaly relative to the intrusion using PV inversion.

We use the PV inversion method of Davis and Emanuel (1991; hereafter DE91). Here we give only a brief description of this method. DE91 developed a technique to perform PV inversion using the Charney balance condition, which is weakly nonlinear and generally satisfied for flows with small curvature and small Rossby number. The geopotential Φ and streamfunction ψ are related by neglecting the divergent and vertical components of the wind.

Static stability and CAPE are related to the balanced dynamical fields Φ and ψ from the PV inversion, through the hydrostatic relationship $\partial\Phi/\partial\pi = -\theta$, where $\pi = c_p(p/p_0)^\kappa$ is the Exner function serving as the vertical coordinate. To find the "balanced vertical motion field" that is consistent with the balanced horizontal winds, we opt to work with the **Q**-vector form of the ω equation (e.g., Morgan 1999) and included the β effect (Bluestein 1992):

$$\mathcal{L}(\omega) = -2\boldsymbol{\nabla}\cdot\mathbf{Q} - \beta\frac{\partial\theta}{\partial x}, \tag{3}$$

where

$$\mathcal{L} = S\nabla^2 + \frac{f_o^2}{\gamma}\frac{\partial^2}{\partial p^2}, \quad S = -\frac{T}{\theta}\frac{\partial\bar{\theta}}{\partial p}, \quad \gamma = \frac{R}{p}\left(\frac{p}{p_o}\right)^\kappa, \tag{4}$$

$$\mathbf{Q} = \left[-\frac{d\mathbf{v}}{dx}\cdot\boldsymbol{\nabla}\theta, -\frac{d\mathbf{v}}{dy}\cdot\boldsymbol{\nabla}\theta\right], \tag{5}$$

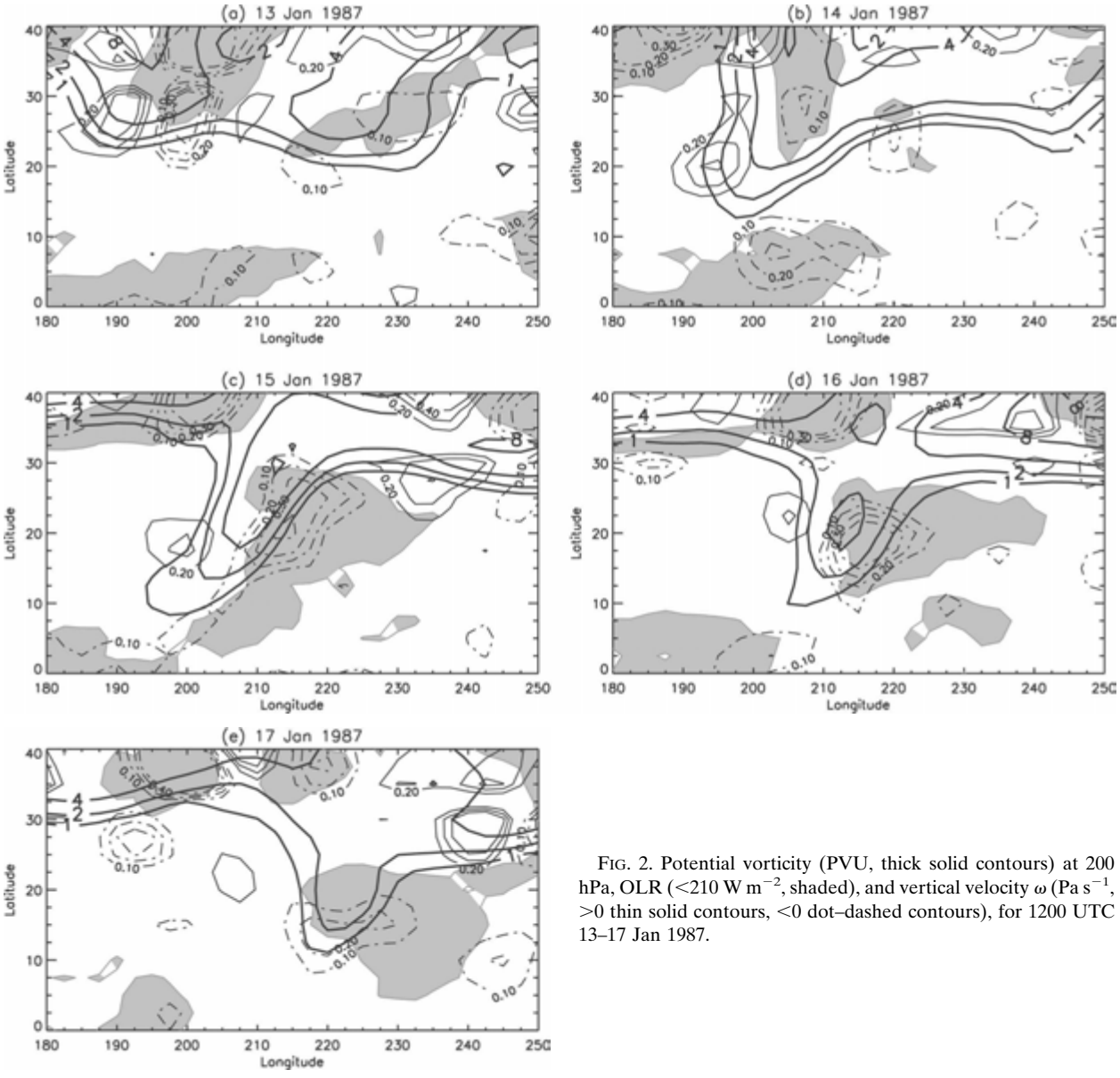

FIG. 2. Potential vorticity (PVU, thick solid contours) at 200 hPa, OLR (<210 W m^{-2}, shaded), and vertical velocity ω (Pa s^{-1}, >0 thin solid contours, <0 dot–dashed contours), for 1200 UTC 13–17 Jan 1987.

$R = 287$ J kg^{-1} K^{-1}, $\kappa = R/c_p$, $c_p = 1004.5$ J kg^{-1} K^{-1}, $\beta = df/dy = 2\Omega \cos\phi/a$, a is the average radius of the earth, Ω is the earth's rate of rotation, and $\mathbf{v} = (u, v)$ is the horizontal wind field. Notice that $T/\theta = (p/1000)^{\kappa}$, and therefore $\mathcal{L}$ is linear despite the θ dependency on the right-hand side of Eq. (3). The **Q** vector is calculated using the balanced fields from PV inversion. In the above ω–**Q** vector formulation, there is no diabatic or frictional forcing for the vertical motion, that is, a particle initially on an isentropic surface will remain on this surface. This approach provides a quantitative estimate of the vertical motion as the system evolves, although this assumption does not hold for the entire time span of the system evolution.

We applied the above inversion method to the intrusion on 15 January 1987. The method was applied to the 0°–60°N, 150°–260°E region using NCEP–NCAR reanalysis geopotential field and its associated geostrophic streamfunction as boundary conditions. We found that there is a very good agreement in the geopotential fields at all levels between the inverted (balanced) fields and reanalysis data (not shown). Discrepancies in the wind field are of the same order of magnitude as found by other studies for midlatitudes (e.g., Agusti-Panareda et al. 2004). Overall, the inversion method was able to reproduce the main pattern, magnitude, and position of the centers of maxima and minima of wind and geopotential fields.

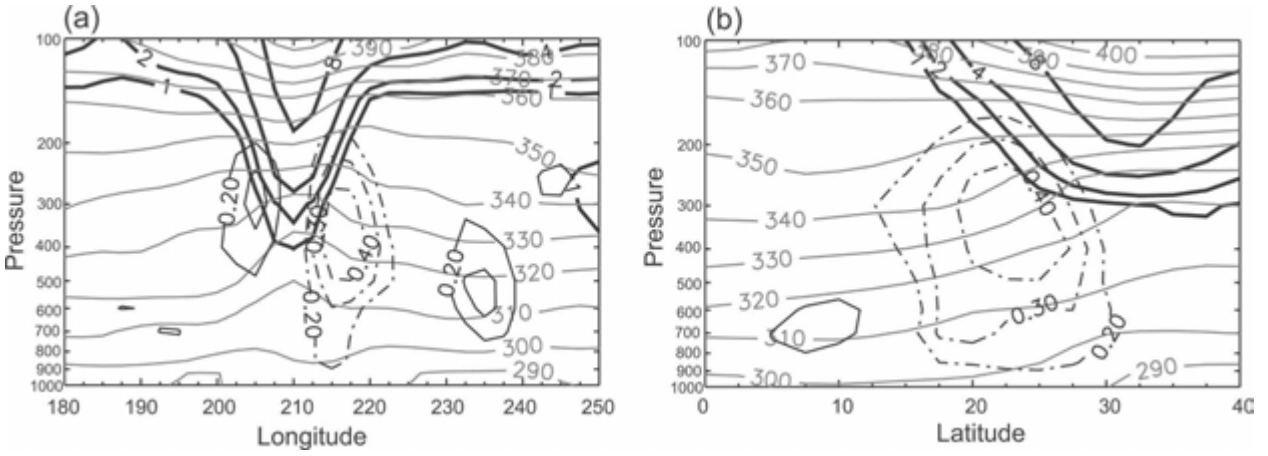

FIG. 3. Vertical cross section of θ (K, gray lines), PV (PVU, thick lines), and vertical velocity ω (Pa s^{-1}, >0 thin black solid, <0 dot–dashed) at (a) 25°N and (b) 215°E, at 1200 UTC 15 Jan 1987.

Because the inversion described above is two-dimensional, it is necessary to find the corresponding vertical motion that is consistent with the horizontal flow. The vertical velocities were then calculated from the inverted fields using Eq. (3). Figures 4a–c show a comparison between the vertical velocity ω at 500 hPa from reanalysis data (Fig. 4a), inverting Eq. (3) using **v** and T from the reanalysis to calculate **Q** (Fig. 4b), and inverting Eq. (3) using balanced **v** and T from PV inversion (Fig. 4c). There are noticeable differences between reanalysis ω and inverted ω [obtained by solving Eq. (3)]. The upward velocity (dash–dotted contour) is weaker and the downward velocity (solid) is stronger than the reanalysis data. These differences are not surprising because diabatic heating is not included in the formulation of the ω equation and convective forcing is also not completely accounted for. The vertical velocity ω obtained here represents the instantaneous vertical velocity of the system as it adjusts itself to be in quasi-geostrophic balance. Although ω in Fig. 4b is not quantitatively accurate it provides the correct position and pattern of upward and downward motions, and the correct order of magnitude of the velocity. Figure 4c shows the solution of Eq. (3) using the balanced horizontal wind and temperature fields to calculate the forcing term, and the resulting ω is still similar to that shown in Fig. 4b. We will use values calculated from the ω equation to obtain a rough *estimate* of the contribution of intrusion on the vertical field relative to the total field.

To address the issue of attribution we first defined the basic state as a 5-day mean around the day of the intrusion (i.e., from 13 to 17 January), and the upper-level PV anomaly (q'_U) associated with the intrusion as the perturbation relative to this mean in the layer between 400 and 100 hPa, which was the layer where the anomaly was equal to or greater than 1 PVU. Here, attribution is used in the same sense as in Bishop and Thorpe (1994) and Thorpe (1997). We aim to determine the changes in the thermodynamical fields that are induced as a response (are "attributable") to the upper-level anomaly.

Figure 5a compares the evolution of the static stability $\mathcal{S}$ calculated using the temperature from PV inversion of total PV field (solid curve) with the contribution due to q'_U only (dashed curve), at 20°N, 212.5°E. Both curves show a steady decrease of static stability up to 16 January, indicating that a large component of the decrease in static stability is attributable to q'_U. The time variation of perturbation static stability averaged over 48 h before 1200 UTC 15 January at the grid point shown is of -7.8×10^{-4} K m^2 kg^{-1} day^{-1}, while the decrease resulting from q'_U is of -4.3×10^{-4} K m^2 kg^{-1} day^{-1}, that is, 55%. However, if we take an average over 17.5°–22.5°N, 210°–215°E the overall decrease is -4.5×10^{-4} K m^2 kg^{-1} day^{-1}, while the decrease related to q'_U is -7.7×10^{-5} K m^2 kg^{-1} day^{-1}, that is, the contribution of q'_U is of over 100% of the total decrease.

A similar comparison of CAPE, for the same location, is shown in Fig. 5b. The calculation of CAPE depends on both temperature and moisture fields. Moisture effect is incorporated in the calculation of virtual potential temperature and also determines, together with temperature, the lifting condensation level. Therefore, the relationship between CAPE and CAPE resulting from q'_U is nonlinear because of CAPE dependency on both temperature and moisture. Unfortunately, PV inversion cannot determine the amount of moisture directly associated with a particular distribution of PV. We therefore have to use the moisture field from the reanalysis in our calculations of CAPE. The dashed

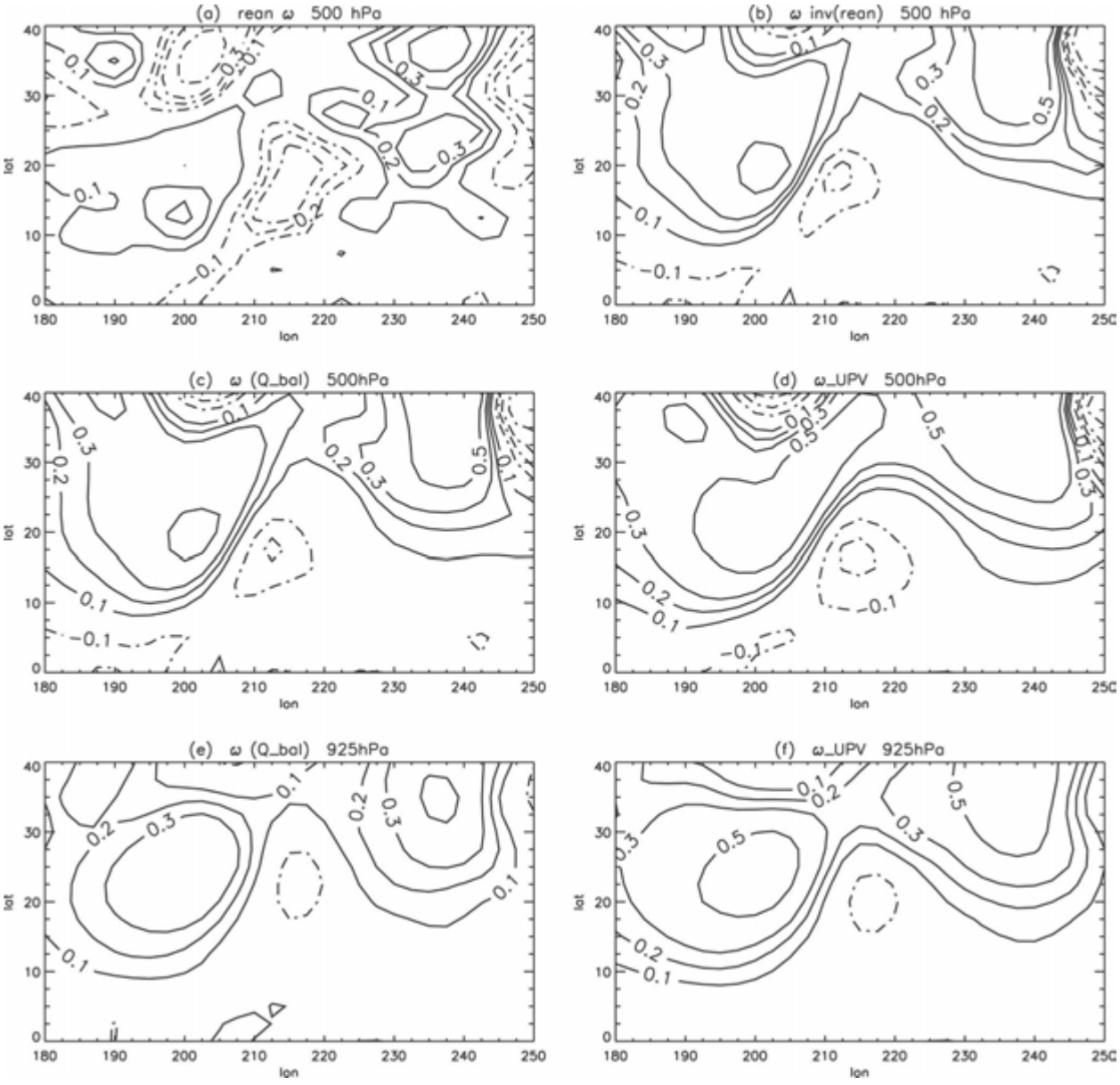

FIG. 4. Vertical velocity ω (Pa s^{-1}) given by (a) NCEP–NCAR reanalysis data; (b) solving the **Q** vector form of the ω equation [Eq. (3), where **Q** is calculated using (u, v, T) from reanalysis data]; same as (b), but using balanced **v**, T from PV inversion to calculate **Q** at (c) 500 and (e) 925 hPa; and (d), (f) ω associated with q'_U. See section 2 for details of calculation.

curve in Fig. 5b shows the contribution of q'_U to CAPE (CAPE$'_U$), calculated using T from the PV inversion and water vapor mixing ratios from the NCEP–NCAR reanalysis. The evolution and magnitude of CAPE$'_U$ is similar to that of "total" CAPE, with enhanced values between 0000 UTC 15 January and 0000 UTC 16 January. The contribution of q'_U through changes in temperature is about 80% of the total CAPE. This result is in line with those found by Juckes and Smith (2000) who showed, using a theoretical model, that upper-level troughs both in the tropics and midlatitudes can cause an increase in CAPE, with the increase being larger for stronger and/or broader troughs.

An issue with the above analysis of CAPE is that it considers only the contribution of changes in T. To examine the sensitivity of CAPE to changes in moisture and temperature, sensitivity calculations (for the period of 13–17 January 1987) were performed where either T or water vapor were hold constant. The dotted curve in Fig. 5b shows CAPE calculated using the time-mean

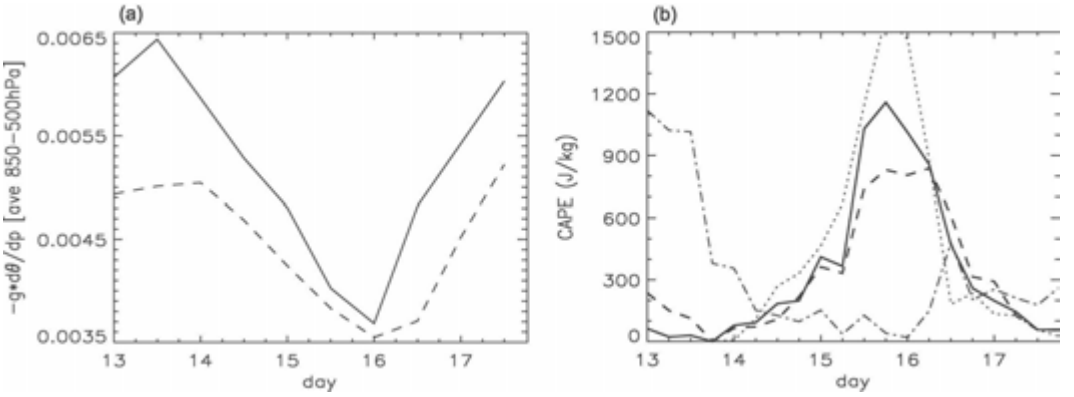

FIG. 5. Time series of (a) dry static stability $\mathcal{S}$ ($=-g\partial\theta/\partial p$ averaged in the layer of 850–500 hPa, in K m^2 kg^{-1}), and (b) CAPE (J kg^{-1}) for the period of 13–17 Jan 1987 at 20°N, 212.5°E, calculated using results from PV inversion; total field (solid line) and sum of contribution of q'_U and average $\mathcal{S}$ or CAPE (dashed line). In (b), dotted curve corresponds to CAPE calculated using constant 5-day-averaged mixing ratio profile, and dash–dot curve using constant 5-day averaged temperature profile; see text for details.

water vapor mixing ratio profiles, but the original time-varying temperature fields, whereas the dot–dashed curve shows CAPE calculated using the time-mean temperature profile and time-varying water vapor. For a fixed temperature the signal of CAPE is strong in the early part of the event but does not show any buildup prior to the onset of convection, whereas for a fixed mixing ratio there is a very strong signal of CAPE, with the pattern and intensity resembling that of CAPE calculated using the actual profiles of T and mixing ratio (solid curve in Fig. 5b). Therefore, for this event CAPE is more sensitive to the temperature changes than to the moisture changes.

The last dynamical variable we examine is the vertical velocity ω. Figures 4c,e show ω obtained by inverting Eq. (3) using the total balanced field, while Figs. 4d,f show the contribution of q'_U to ω (i.e., ω'_U) for the levels of 500 and 925 hPa, calculated as explained in section 3. This figure shows that q'_U contributes to virtually all of the balanced upward motion field ahead of the intrusion in the lower- and midlevels of the atmosphere. Note that, as shown in Figs. 4a,c, the balanced ω is only around 66% of the total ω in the region of interest. Calculation of the contribution of q'_U averaged over the area of 15°–20°N, 212.5°–217.5°E show that the vertical ascent at 925, 700, and 500 hPa are exclusively attributable to the upper-level intrusion.

The above analysis shows that the upper-level PV intrusion contributes ~60% or more in the changes of static stability and CAPE and ~100% of the changes in the balanced ascent. The strength of this analysis is the PV invertibility and attribution concepts. However, there are several caveats: The inversion assumes Charney balance; the vertical velocity was calculated using the **Q** vector, which is based on the quasigeostrophic theory; and CAPE change resulting from moisture change could not be accessed by PV inversion. In an effort to confirm the crucial importance of PV intrusion on these variables, we use numerical model simulations and isolate the contribution of the upper-level anomaly to the same fields as above and compare the results.

4. Numerical model simulations

In the previous section we presented a quantitative estimate of the effect of upper-level PV anomalies associated with an intrusion on dynamical and thermodynamical fields characterizing convection. These estimates showed that intrusions play a key role in destabilizing the lower atmosphere, building up CAPE, and promoting vertical ascent. However, as discussed above, this analysis has some limitations because it was based on PV inversion. In this section, we use a mesoscale model to further quantify the role of key quantities (PV, latent heat) in the development of convection. This is achieved by performing numerical simulations where the upper-level PV anomalies or latent heat release are removed. Comparison of these with simulations that include upper-level PV anomalies and latent heat release then enable the impact of different factors to be directly determined.

a. Model description and setup

We use version 3 of the fifth-generation Pennsylvania State University–NCAR Mesoscale Model (MM5; Dudhia 1993; Grell et al. 1995). In our simulations we use a single domain covering the region of 0.22°–44.10°N,

179.9°–254.1°E, with horizontal resolution of 50 km. The top of the model is at 50 hPa, with 31 unevenly spaced σ levels with slightly more in the boundary layer and the upper troposphere.

MM5 requires the input of geopotential height, horizontal wind, temperature, relative humidity, sea level pressure, sea surface temperature, and snow cover data for the initial and boundary conditions. NCEP–NCAR reanalysis data are used for these initial and boundary conditions. In the simulations presented below balanced geopotential and wind fields are used rather than the original NCEP–NCAR reanalysis. These balanced fields were obtained by PV inversion of the NCEP–NCAR reanalysis data as described in section 2. The area used in the PV inversion was 0°–60°N, 150°–260°E (25×45 grid points). Balanced fields were used to eliminate undesired high-frequency waves, such as gravity waves, from the initial conditions, and also so that clean comparisons could be made between simulations with and without the upper-level PV anomalies (see further discussion below).

MM5 can be run with several different options for cumulus parameterizations, and simulations were performed with several of these options. Specifically, simulations were performed using the Betts–Miller, Anthes–Kuo, or Kain–Fritsch convective parameterizations, or with the "no cumulus parameterization" option. The sensitivity of the simulations to the choice of cumulus parameterization is described in the next subsection.

The other physical parameterizations were the same in all simulations, and we used the simple ice microphysics scheme (Dudhia 1993), cloud–radiation scheme for radiation (Dudhia 1993), five-layer soil model for surface scheme, and the Medium-Range Forecast (MRF) planetary boundary layer (PBL) scheme (Hong and Pan 1996).

In some simulations we wish to switch off latent heat release. This was done using the "fake dry" option within MM5, in which water vapor is transported as a passive tracer with no phase changes. This option is possible in MM5 only when run with the no-cumulus-parameterization option.

b. Control run

We first describe the "control" simulation for the intrusion case of 13–17 January 1987. As described above we wish to compare runs where either the upper-level PV anomaly or latent heat release is removed. The need to do these simulations places some constraints on the specifications of the control simulation.

In runs where the upper-level PV anomaly is removed, initial and boundary conditions for geopotential height, wind, and temperature fields that are consistent with the "altered" PV distribution are determined using PV inversion. This requires assuming a balance condition (see details below). Because balanced initial and boundary fields are used in this perturbation run we also use the same balance for the control simulation. This means that differences between the control and PV-removed simulation can be attributed to differences in the PV distribution, and are not due to differences between balanced and unbalanced initial conditions.

To perform simulations with no latent heat release we use the fake dry option within MM5 in which water vapor is transported as a passive tracer with no phase changes. As described above, this option is only available when there is no cumulus parameterization. Hence, to again be consistent between simulations and allow meaningful comparisons we make the same choice, that is, a no cumulus parameterization, in the control simulation.

In summary, the control simulation uses balanced NCEP–NCAR reanalysis fields as the initial and boundary conditions and no convective parameterization, with the remaining setup as described in the previous subsection. This allows clean comparisons between the control and perturbation simulations described below.

The initial time for the run was 0000 UTC 13 January 1987, and the model was allowed to run for 120 h, that is, until 0000 UTC 18 January 1987. The time sequence of PV and OLR for the period of 1200 UTC 13–17 January 1987 for this control run is shown in Fig. 6. Comparison with reanalysis (Fig. 2) shows that PV evolution is fairly well simulated. As in the reanalysis, a tongue of high PV develops on 14 January, reaches as far south as 10°N on 15 January, and has decayed by 17 January. Perhaps the major disagreement in the PV fields is the downstream side of the trough where the simulation cannot reproduce the sharper "kink" that can be seen in the PV field from the reanalysis.

The general features in the observed OLR are also captured in the simulation. There is a region of low OLR ahead of the PV tongue, which moves eastward with the PV tongue. The agreement between the simulated and observed OLR is not as good as for PV. In particular, the area of simulated low OLR is smaller than observed (especially on 15 January). Also, the simulation does not produce the observed region of low OLR on the equator around 180°–200°E. The region of equatorial low OLR is associated with the ITCZ and is not captured in the model because of the limited area of the model (with a southern boundary at approximately 0.22°N and western boundary at 180°E). Blow-off cirrus from the equatorial convection may contribute to some

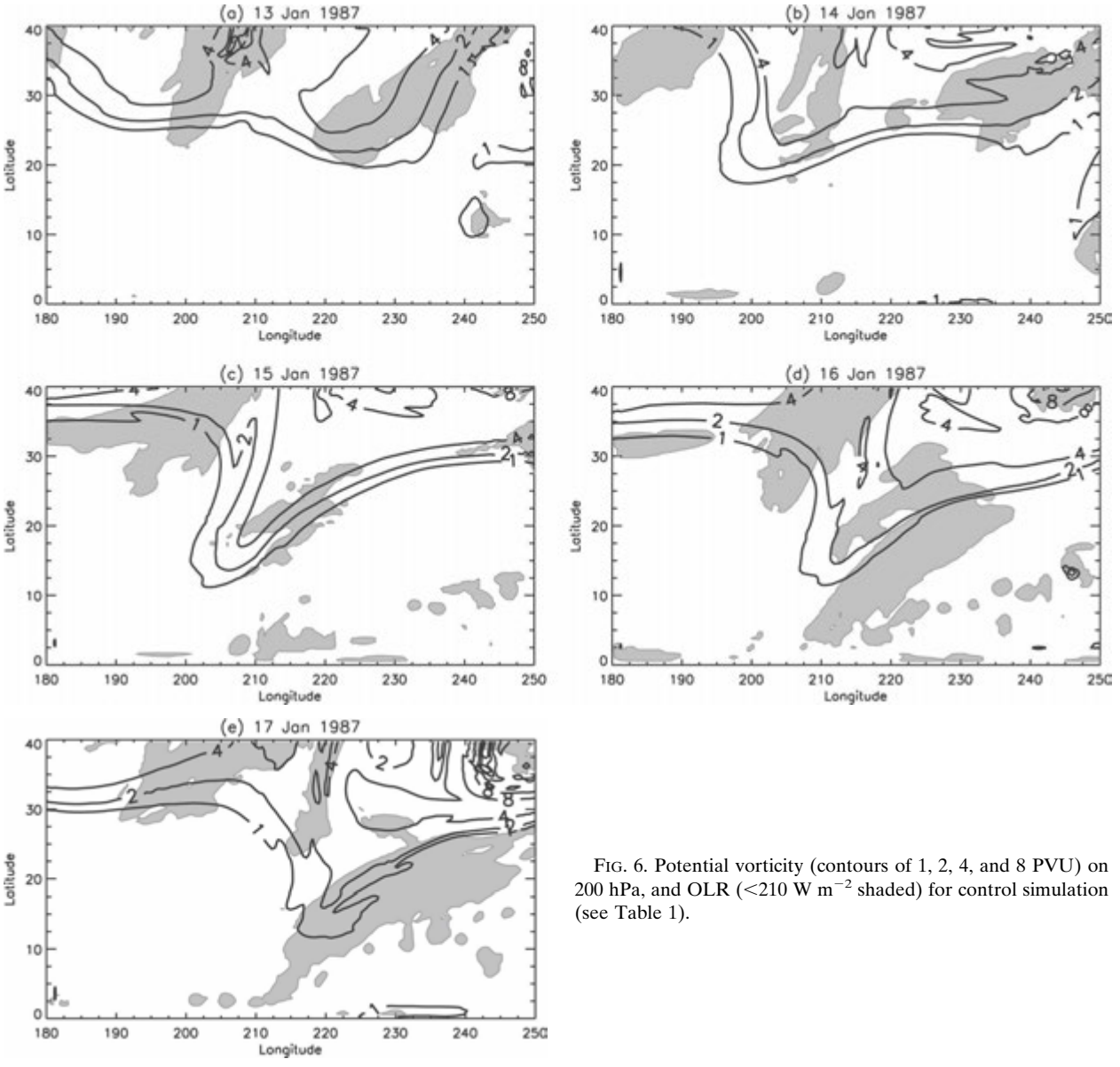

FIG. 6. Potential vorticity (contours of 1, 2, 4, and 8 PVU) on 200 hPa, and OLR (<210 W m^{-2} shaded) for control simulation (see Table 1).

of the low OLR north of the equator, and lack thereof in the model may contribute to the smaller region of low OLR ahead of the intrusion. Although there are the above model–data differences, the model does simulate the required key feature of low OLR downstream of the PV tongue.

There is also general agreement between the simulations and reanalysis in the ascent and enhanced CAPE in the region of low OLR (not shown). Consistent with the differences between simulated and observed OLR, the simulated region of ascent is smaller and more fragmented than that in NCEP–NCAR reanalysis and the maximum CAPE is located west of that calculated using NCEP–NCAR reanalysis.

The major deficiency in the control simulation is that there is insignificant precipitation. Having no precipitation is clearly unrealistic, and is due to the lack of a cumulus parameterization. Not using a cumulus parameterization means that any precipitation in the model must occur at the 50-km grid scale (and if precipitation does occur it probably occurs in an unrealistic manner). Given that precipitation occurs in reality and is missing from control and other runs with no cumulus parameterization, it is likely that the latent heat release is underestimated in these runs. Hence, some caution should be applied when interpreting the impact of latent heat release in the simulations presented below.

Note that simulations have been performed using dif-

TABLE 1. MM5 simulations presented. All runs have same set up as the control ("CNTL") run except for changes listed.

Run	Description
CNTL	Balanced initial and boundary conditions, no cumulus parameterization, 50-km resolution
UPV	As in CNTL except no latent heat release
LH	As in CNTL except no PV anomaly in initial and boundary conditions
OTHR	As in CNTL except no PV anomaly in initial and boundary conditions and no latent heat release

ferent cumulus parameterizations, with the same initial and boundary conditions as the control run. Significant precipitation did occur in some of these simulations, for example, simulations using Betts–Miller and Anthes–Kuo convective schemes resulted in accumulated precipitation larger than 3 cm nearly coincident with low OLR regions. However, the structure and evolution of PV, low OLR, and CAPE are essentially the same as in the control run in these simulations (Funatsu 2005). In other words, the cumulus parameterization and precipitation does not change the location or timing of the buildup of CAPE, the decrease in static stability and OLR, or the increase in vertical ascent.

Although there are differences in details between the simulation and observations, the main features in which we are interested—development of PV intrusion with ascent, enhanced CAPE, and low OLR ahead—are simulated. This gives us confidence that we can use MM5 simulations to examine the impact of different factors on the initiation of convection.

c. *Factor separation simulations*

To evaluate the contributions of the upper-level PV anomaly (q'_U) and latent heat to changes in CAPE, ω, and $\mathcal{S}$, we perform the following four simulations (Table 1):

- the control simulation described above (CNTL),
- a simulation with q'_U but no latent heat (UPV),
- a simulation with latent heat but no q'_U (LH), and
- a simulation without q'_U or latent heat (OTHR).

In all four simulations balanced fields are used for initial and boundary conditions and there is no cumulus parameterization. In the LH and OTHR runs, the upper-level PV anomaly q'_U was "removed" from the initial and boundary conditions and PV inversion of the "altered" distribution (mean field replacing the PV anomaly) was performed. The resulting balanced geopotential, wind, and temperature fields were then used as the initial and boundary conditions for those runs. Using the balanced fields was a necessary measure to minimize spurious results that could arise due to nonphysical gradients in the fields where the anomaly was removed. This approach provides results that are self-consistent and thus the comparison between different runs is meaningful. In the UPV and OTHR runs, latent heat release was removed (i.e., water vapor was transported as a passive tracer with no phase changes) using the fake dry option in MM5.

The PV and OLR on 1200 UTC 15 January 1987 for runs UPV, LH, and OTHR are shown in Fig. 7. Comparing with the corresponding fields from the CNTL simulation shown in Fig. 6 it is clear that subtropical low OLR is related to the presence of the intrusions because there is no signal of OLR when q'_U is removed. This supports the hypothesis that the upper-level PV anomaly is the dominant factor causing the convection and low OLR.

The differences in the thermal structure and vertical motion between the simulations are quantified in Fig. 8, which shows the time evolution of OLR, dry static stability $\mathcal{S}$, CAPE, and vertical velocity $\omega(= dz/dt)$. The values are averaged over $5^\circ \times 5^\circ$ regions because, for most of these parameters, there is a lot of finescale structure and an area average is more representative than a point value. Also, the regions used for each parameter differ slightly (see top of each plot), and were chosen such that the region includes the extrema of the given field.

To better isolate the contributions of the two factors—latent heat and the upper-level PV anomaly (q'_U)—we use the "factor separation method" of Stein and Alpert (1993). Using this method, the part of a field f (e.g., OLR, vertical velocity) solely due to the q'_U is given by

$$\hat{f}_{q'_U} = f_{\mathrm{UPV}} - f_{\mathrm{OTHR}},$$

where f_{UPV} is the field from the UPV simulation and f_{OTHR} the field from the OTHR simulation. Similarly, the contribution solely due to latent heat is

$$\hat{f}_{\mathrm{LH}} = f_{\mathrm{LH}} - f_{\mathrm{OTHR}},$$

and the contribution due to the interaction between q'_U and latent heat is

$$\hat{f}_{\mathrm{INTR}} = f_{\mathrm{CNTL}} - f_{\mathrm{UPV}} - f_{\mathrm{LH}} + f_{\mathrm{OTHR}}.$$

In the above calculations it is assumed that there is no interaction with the background field [a modification of this method to evaluate the potential nonlinearity of the basic system and the response of the model to the fractional effect of a factor was presented by

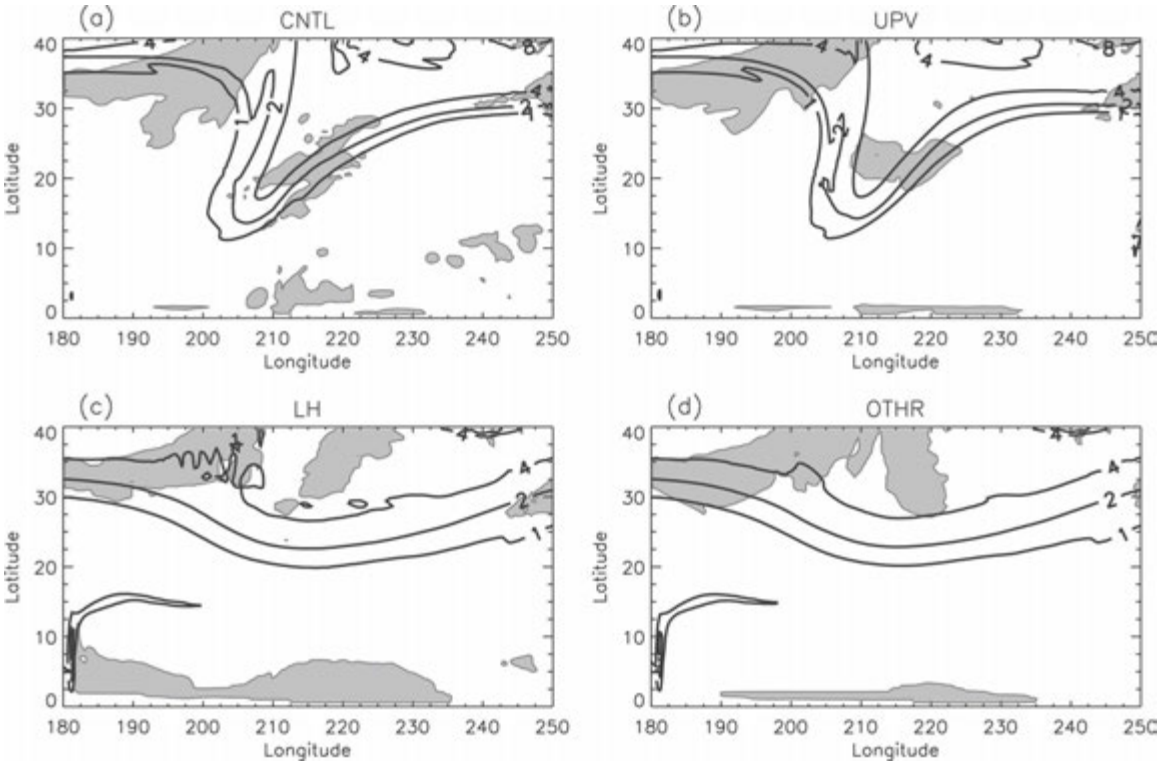

FIG. 7. Same as Fig. 6, on 1200 UTC 15 Jan 1987, except for (a) CNTL, (b) UPV, (c) LH, and (d) OTHR.

Krichak and Alpert (2002), but is not explored here]. This was also assumed in the analyses performed in section 3; therefore, the results obtained from this method may be compared to the PV inversion analyses.

Figure 9 shows the evolution of the same fields as Fig. 8, except for the individual contributions of q'_U, latent heat, and their interaction determined using the factor separation method, that is, $\hat{f}_{q'_U}$, $\hat{f}_{\mathrm{LH}}$, and $\hat{f}_{\mathrm{INTR}}$.

Figure 8a shows that the OLR from run UPV closely matches the control run until it reaches the deep convection threshold [around 205 W m^{-2}; e.g., Gu and Zhang (2002)] at 1200 UTC 15 January, while for the remaining runs OLR values remain very high (i.e., no deep convection present) throughout the whole simulation period. The total contribution of q'_U to the decrease in OLR is about -60 W m^{-2} between 0000 and 1200 UTC 15 January, while the interaction term and latent heat contributed with less than -10 W m^{-2} (see Fig. 9a). Only after convection spreads throughout a large area (16 January) is there a large drop in the interaction term.

The variation of the static stability in run UPV also follows that of CNTL prior to the onset of convection, whereas for the other two runs there is only a weak decrease in static stability prior to 15 January (see Fig. 8b). Again, there is a sharp decrease in $\mathcal{S}$ [approximately 10^{-3} K m^2 kg^{-1} $(12\ \mathrm{h})^{-1}$], which is compensated by stabilization by the interaction term (Fig. 9b).

The time sequence of CAPE (Fig. 8c) shows a clear buildup prior to the onset of convection for runs CNTL and UPV. Run LH shows an early CAPE buildup, but a decrease subsequently, while UPV shows a sharp increase immediately before the convection occurs. This suggests that CAPE builds up in response to thermodynamical changes resulting from both latent heat release and the presence of the PV anomaly. It is interesting to see that there is also a small amount of CAPE unrelated to either q'_U and water vapor content. It may be related to changes in the thermodynamical structure resulting from turbulence and/or surface heat fluxes.

To further ascertain that the upper-level PV anomaly was the crucial element to the development of convection rather than surface conditions, we show in Fig. 8e the time sequence of the latent heat flux for the same area and period of that for CAPE (15°–20°N, 207.5°–212.5°E). It is expected that latent heat flux would be enhanced before convection is activated (e.g., Raymond et al. 2006). We see that there is in fact an increase in the LH flux in the 24 h preceding the convection (1200 UTC 14–15 January) for run CNTL; however, run OTHR has a higher latent heat flux but still

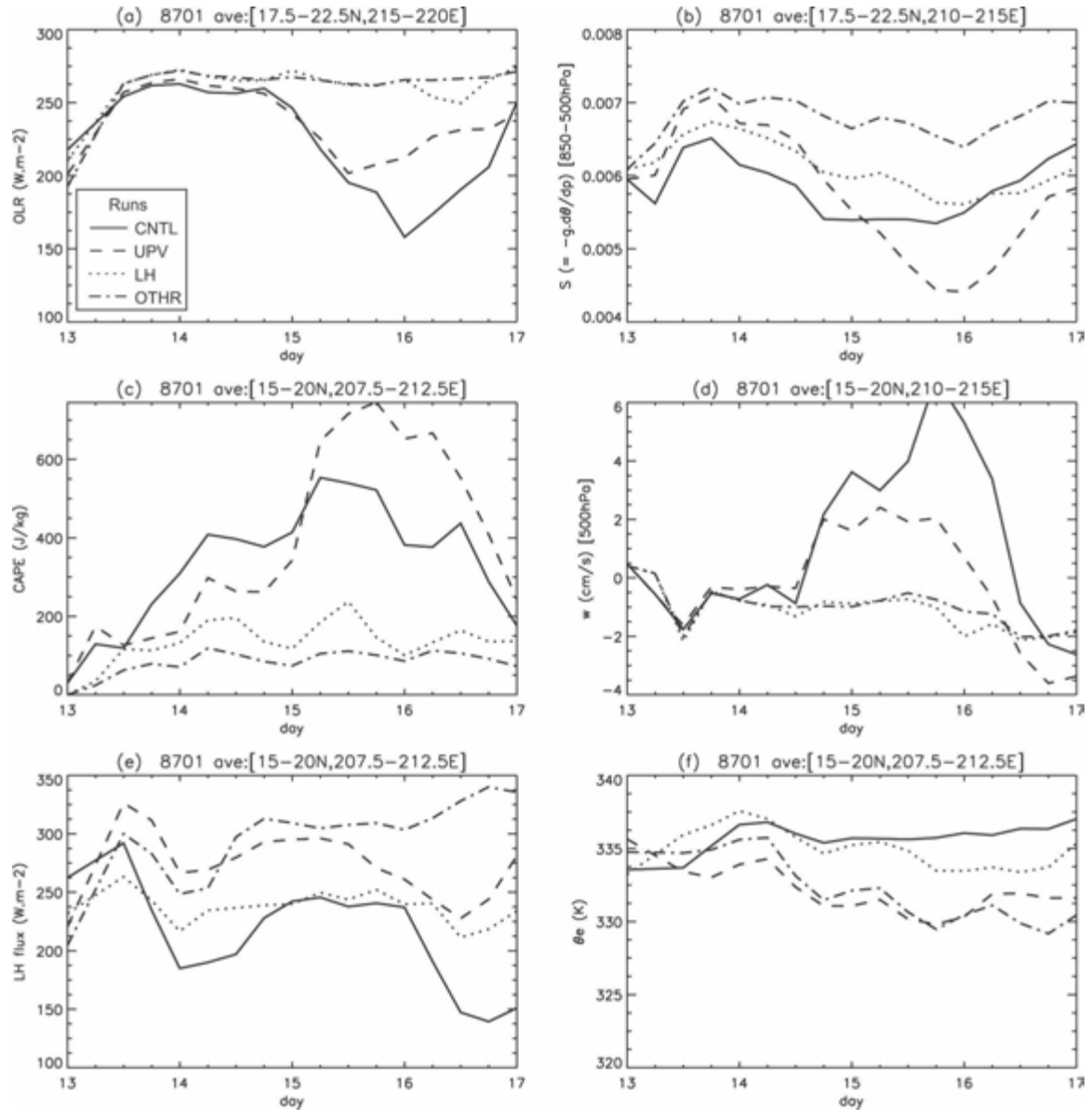

FIG. 8. Time sequence of area-averaged (a) OLR (W m^{-2}), (b) dry static stability $\mathcal{S}$ ($=g\,d\theta/dp$; K m^2 kg^{-1}), (c) CAPE (J kg^{-1}), (d) vertical velocity w ($=dz/dt$; cm s^{-1}), (e) latent heat flux (W m^{-2}), and (f) θ_e (K). Results from MM5 simulation, control run (solid line), including q'_U but no latent heat (dashed line), including latent heat but no q'_U (dotted line), and removing both q'_U and latent heat (dot–dashed line).

did not trigger convection. Run LH had values of latent heat flux very similar to that of CNTL and also failed to produce convection.

These results are corroborated by the evolution of the equivalent potential temperature (θ_e) at 2 m for the same area and period (Fig. 8f). Even though the evolution of θ_e is very similar in runs CNTL and LH, and that latent heat makes the major individual contribution to θ_e (Fig. 9f), run LH did not produce any convection. This supports the hypothesis that surface processes by themselves do not have a sufficient impact in triggering convection, and that the presence of q'_U is of fundamental importance, at least for this case.

The above analysis of the MM5 simulations shows that the upper-level PV makes the dominant contribution to the decrease in OLR and static stability and increase in CAPE between 13 and 15 January. The other factors generally play a much smaller role. Latent heat release alone makes a small contribution in providing energy for convection in the early period and it

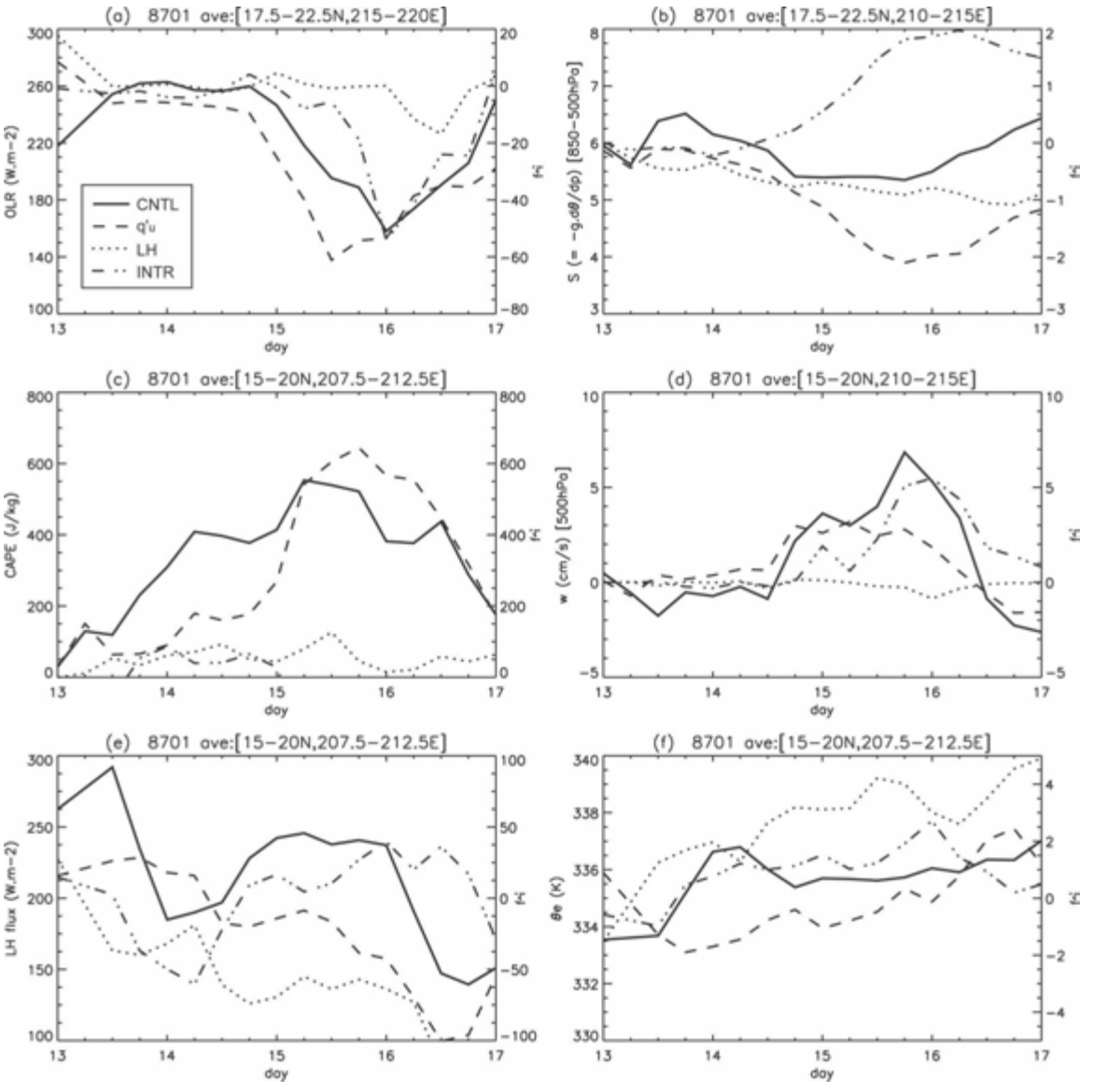

FIG. 9. Time sequence of area-averaged (a) OLR (W m^{-2}), (b) dry static stability $\mathcal{S}(=g\,d\theta/dp;\times10^{-3}$ K m^2 $kg^{-1})$, (c) CAPE (J kg^{-1}), (d) vertical velocity w $(=dz/dt;$ cm $s^{-1})$, (e) latent heat flux (W m^{-2}), and (f) θ_e (K). Results from MM5 control simulation (dark solid), contribution of q'_U only (dashed line), latent heat only (dotted line), and interaction of q'_U and latent heat (dot–dot–dashed line). The y axis on the left refers to control simulation, while values on the right are for the contributions of each factor.

has negligible or negative contribution to vertical ascent. The interaction of q'_U and LH makes a large contribution to the upward vertical motion (57% at 500 hPa), but does not contribute at all to CAPE buildup. Factors unrelated to either q'_U and LH contribute around 22% to the buildup of CAPE prior to convection but at the same time cause relative stabilization of the atmosphere and have a negative contribution to vertical ascent. We note again that the impact of LH may be underestimated in the above analysis due to the lack of precipitation in the simulations. However, this is unlikely to change the dominance of the contribution due to the upper-level PV.

d. Comparison with results of PV inversion

The model results discussed can be compared with the PV inversion analysis presented in section 3. This comparison is only possible for the contribution due to q'_U because this is the only contribution inferred using the PV inversion technique. Both the PV inversion and the MM5 simulations show that the contribution of q'_U to CAPE increases with time, and is dominant in the 24

TABLE 2. Relative contributions (%) of q'_U to CAPE, local tendency of $\mathcal{S}$, and vertical velocity, for the areas indicated in brackets. Contribution for CAPE is the average of 36 h before 1200 UTC 15 Jan 1987, and for $\partial\mathcal{S}/\partial t$ is the average of 48 h before the same date. Vertical velocity (ω for PV inversion, w for MM5 results) is at 500 hPa.

Parameter	PV inversion	Model
CAPE	(20°N, 212.5°E) 56	(15°–20°N, 207.5°–212.5°E) 62
$\partial\mathcal{S}/\partial t$	(17.5°–22.5°N, 210°–215°E) 100	(15°–20°N, 210°–215°E) 72
Vertical velocity	(15°–20°N, 212.5°–217.5°E) 100	(15°–20°N, 210°–215°E) 61

h preceding the onset of convection. Also, q'_U causes a decrease in static stability prior to convection, and vertical ascent in the midtroposphere at the leading edge of the PV intrusion.

Table 2 compares the relative contributions of q'_U to CAPE, to the local tendency of $\mathcal{S}$, and to the vertical velocity for the PV inversion and the model simulations. The compared regions are not exactly the same, but the comparison is still justified because, in both cases, the region used is representative of the region of maximum vertical ascent, maximum cape, and minimum OLR.

Given the deficiencies in the control simulations (i.e., model–data differences), Table 2 shows reasonable agreement between the PV inversion and MM5 simulations. The relative contribution of q'_U to CAPE for the 36 h prior to the convection is very similar for the model results (62%) and PV inversion (56%). There are larger differences between PV inversion and model calculations for local tendency of the static stability: The PV inversion yields a contribution by q'_U of 100%, whereas the model calculations indicate a smaller contribution of around 70%. The smaller contribution in the model calculations is likely related to the fact that the vertical penetration of PV tongue was not as strong in the simulation results, resulting in lesser influence in the lower levels. There is a similar difference between PV inversion and model calculations for the contribution to the vertical velocity, which could also be related to the vertical penetration; although some of the difference is likely because the vertical velocity was calculated using the **Q** vector, which is based on the quasigeostrophic theory, in the PV inversion.

5. Additional cases

A similar analysis, including the PV inversion of the NCEP–NCAR reanalysis and MM5 simulation, was performed for four other cases of stratospheric intrusion in the Pacific region: 12 February 1991, 16 January 1997, 23 January 1999, and 28 January 2003 (Funatsu 2005). All of these events penetrate into the deep tropics (PV $>$ 1.75 PVU south of 12°N at 200 hPa), but differ in their vertical penetration. The February 1991 event has a signal as deep in the atmosphere as in the case of January 1987, but the other events are shallower. In the January 1987 and February 1991 events the 1-PVU anomaly reaches around 400 hPa, while in the other cases it reaches only 300 hPa (not shown).

Qualitative analysis of the data for these events shows destabilization and upward vertical velocity ahead of the intrusion and CAPE accumulation prior to convection, as in the January 1987 event (section 2). The quantitative results from PV inversion (as in section 3) vary with intensity and vertical depth of the PV anomaly, but there is a consistent pattern of CAPE accumulation and decreasing static stability, which is mostly due to the upper-level PV anomaly prior to the outbreak of convection. The contribution of q'_U to CAPE through changes in the temperature before the onset of convection was larger than 50%, while the rate of destabilization was higher than 90% for the 48 h before the deep penetration of the intrusion into the tropics. Estimates of vertical velocity ω show that when the convection was fully developed there was a strong component of the upward vertical velocity due to the PV anomaly, whenever the anomaly was relatively strong.

MM5 simulations were performed for the above cases using the same methodology described in section 4, and the relative contributions of q'_U, latent heat, and their interactions to the simulated total fields were calculated. The simulation results show a dependency on the depth of penetration. The results for the vertically deep intrusion (February 1991) were similar to that shown above for the January 1987 event, with q'_U clearly the dominant factor in contributing to the decrease in OLR and static stability and buildup of CAPE.

For the shallower cases (January 1999, January 1997, and January 2003), the upper-level PV anomaly associated with the intrusion is still a necessary feature for convection to occur, but there is less dominance of q'_U. For the January 1999 event the q'_U contribution was dominant over the other components, except for the buildup of CAPE, where the LH contribution was dominant. In the January 1997 and January 2003 events, both q'_U and its interaction with latent heat made contributions to the decrease in OLR and static stability, and buildup of CAPE. For these events the *interaction* of q'_U and latent heat was of crucial importance for lowering OLR. In fact, for these events the simulations

with q'_U only (as well as the LH and OTHR) did not yield areas with significantly low OLR.

6. Conclusions

In this study we have examined the connection between potential vorticity (PV) intrusions into the tropical upper troposphere and deep convection over the east Pacific, using NCEP–NCAR reanalysis data, PV inversion, and mesoscale model simulations. Our primary focus was on a previously studied event that occurred in January 1987 (Kiladis and Weickmann 1992b; Waugh and Funatsu 2003), although several other events were also examined.

Analysis of NCEP–NCAR reanalysis and satellite measurements of OLR showed a consistent pattern in all events of increased cloudiness, reduced static stability, enhanced CAPE, and upward vertical motion at the leading edge of the PV intrusion prior to the outbreak of convection. The link between upper-level PV and the convection was quantified using PV inversion. These calculations showed that the upper-level PV anomaly associated with the intrusion makes the dominant contribution to the changes in the quantities that characterize convection. For example, in all events the upper-level PV contributes over 90% of the change in static stability prior to convection. These results are consistent with theoretical expectations and support the hypothesis (Kiladis 1998) that the upper-level PV initiates and supports convection by destabilizing the lower troposphere and causing upward motion ahead of the tongues.

The relative contributions of the upper-level PV anomalies and latent heat were further examined using the fifth-generation Pennsylvania State University–NCAR Mesoscale Model (MM5). A series of MM5 simulations with PV intrusion and/or latent heat removed were performed to isolate the contributions of the different factors. Increased cloudiness (i.e., low OLR) did not occur over the tropical eastern Pacific when the intrusion was removed from the simulations, confirming that the intrusions cause the convection. Furthermore, analysis of the relative contribution of different factors showed, consistent with the PV inversion calculations, that the upper-level PV anomaly is the dominant factor causing the decrease in OLR and static stability, and increase in CAPE and upward vertical velocity. The latent heat effect by itself made only a minor contribution, but the interaction term between PV and latent heat became more important as the convection developed.

The combined occurrence of intrusions and convection described above is potentially very important for stratosphere-to-troposphere exchange and the composition of the tropical upper troposphere. The intrusions transport high-ozone, low-water vapor stratospheric air into the subtropical middle–upper troposphere (e.g., Scott et al. 2001; Waugh and Funatsu 2003; Cooper et al. 2005), while the convection ahead of the intrusion transport low-ozone, high-water vapor air into the upper troposphere (Waugh 2005). Furthermore, the convection contributes to the erosion and decay of the intrusion, and mixing of stratospheric and tropospheric air (Langford and Reid 1998; Cooper et al. 2005). The net impact of above processes on the subtropical moisture and ozone distributions is, however, unknown, and is an area of future research.

Another area worth pursuing is the role intrusions and convection play in possible links between the east and west Pacific. Slingo (1998) proposed a picture in which convection in the western Pacific can induce changes in the East Asian jet, which in turn could amplify Rossby wave disturbances. These waves cause convection in the eastern tropical Pacific, which in turn are hypothesized to excite low-tropospheric easterly waves that propagate back to the west Pacific and contribute to convective activity in this region. It would be of interest to examine whether there is any such link between intrusions and easterly waves.

Acknowledgments. We thank George N. Kiladis for helpful comments and discussion on this manuscript. BMF thanks Cindy Bruyere and Eric Ray for their invaluable assistance with MM5, and Paul Newman for access to NCEP–NCAR reanalysis data. The NOAA spatially and temporally interpolated OLR were obtained from the NOAA–CIRES Climate Diagnostics Center (information online at http://www.cdc.noaa.gov/). This work was supported by grants from NSF and NASA.

REFERENCES

Agusti-Panareda, A., C. D. Thorncroft, G. C. Craig, and S. L. Gray, 2004: The extratropical transition of hurricane *Irene* (1999): A potential-vorticity perspective. *Quart. J. Roy. Meteor. Soc.,* **130,** 1047–1074.

Bishop, C. H., and A. J. Thorpe, 1994: Potential vorticity and the electrostatics analogy: Quasi-geostrophic theory. *Quart. J. Roy. Meteor. Soc.,* **120,** 713–731.

Bluestein, H. B., 1992: *Principles of Kinematics and Dynamics.* Vol. 1. *Synoptic-Dynamic Meteorology in Midlatitudes,* Oxford University Press, 431 pp.

Cooper, O. R., and Coauthors, 2005: Direct transport of midlatitude stratospheric ozone into the lower troposphere and marine boundary layer of the tropical Pacific Ocean. *J. Geophys. Res.,* **110,** D23310, doi:10.1029/2005JD005783.

Davis, C. A., and K. A. Emanuel, 1991: Potential vorticity diagnostics of cyclogenesis. *Mon. Wea. Rev.,* **119,** 1929–1953.

Dixon, M. A. G., A. J. Thorpe, and K. A. Browning, 2003: Layer-wise attribution of vertical motion and the influence of potential-vorticity anomalies on synoptic development. *Quart. J. Roy. Meteor. Soc.,* **129,** 1761–1778.

Dudhia, J., 1993: A nonhydrostatic version of the Penn State–NCAR mesoscale model: Validation tests and simulation of an Atlantic cyclone and cold front. *Mon. Wea. Rev.,* **121,** 1493–1513.

Funatsu, B. M., 2005: Stratospheric intrusions and transient convection in the eastern tropical Pacific. Ph.D. thesis, Johns Hopkins University, 133 pp.

Grell, G. A., J. Dudhia, and D. R. Stauffer, 1995: A description of the fifth-generation Penn State/NCAR mesoscale model (MM5). NCAR Tech. Note NCAR/TN-398+STR, 138 pp.

Gu, G. J., and C. D. Zhang, 2002: Cloud components of the Intertropical Convergence Zone. *J. Geophys. Res.,* **107,** 4565, doi:10.1029/2002JD002089.

Hoerling, M. P., 1992: Diabatic sources of potential vorticity in the general circulation. *J. Atmos. Sci.,* **49,** 2282–2292.

Hong, S.-Y., and H.-L. Pan, 1996: Nonlocal boundary layer vertical diffusion in a medium-range forecast model. *Mon. Wea. Rev.,* **124,** 2322–2339.

Hoskins, B. J., and T. Ambrizzi, 1993: Rossby wave propagation on a realistic longitudinally varying flow. *J. Atmos. Sci.,* **50,** 1661–1671.

——, M. E. McIntyre, and A. W. Robertson, 1985: On the use and significance of isentropic potential vorticity maps. *Quart. J. Roy. Meteor. Soc.,* **111,** 877–946.

——, M. Pedder, and D. W. Jones, 2003: The omega equation and potential vorticity. *Quart. J. Roy. Meteor. Soc.,* **129,** 3277–3303.

Juckes, M., and R. K. Smith, 2000: Convective destabilization by upper-level troughs. *Quart. J. Roy. Meteor. Soc.,* **126,** 111–123.

Kalnay, E., and Coauthors, 1996: The NCEP/NCAR 40-Year Reanalysis Project. *Bull. Amer. Meteor. Soc.,* **77,** 437–471.

Kiladis, G. N., 1998: Observations of Rossby waves linked to convection over the eastern tropical Pacific. *J. Atmos. Sci.,* **55,** 321–339.

——, and K. M. Weickmann, 1992a: Circulation anomalies associated with tropical convection during northern winter. *Mon. Wea. Rev.,* **120,** 1900–1923.

——, and ——, 1992b: Extratropical forcing of tropical Pacific convection during northern winter. *Mon. Wea. Rev.,* **120,** 1924–1938.

——, and S. B. Feldstein, 1994: Rossby wave propagation into the tropics in two GFDL general circulation models. *Climate Dyn.,* **9,** 245–252.

Krichak, S. O., and P. Alpert, 2002: A fractional approach to the factor separation method. *J. Atmos. Sci.,* **59,** 2243–2252.

Lamarque, J.-F., and P. G. Hess, 1994: Cross-tropopause mass exchange and potential vorticity budget in a simulated tropopause folding. *J. Atmos. Sci.,* **51,** 2246–2269.

Langford, A. O., and S. J. Reid, 1998: Dissipation and mixing of a small-scale stratospheric intrusion in the upper troposphere. *J. Geophys. Res.,* **103,** 31 265–31 276.

Liebmann, B., and C. A. Smith, 1996: Description of a complete (interpolated) outgoing longwave radiation dataset. *Bull. Amer. Meteor. Soc.,* **77,** 1275–1277.

Morgan, M. C., 1999: Using piecewise potential vorticity inversion to diagnose frontogenesis. Part I: A partitioning of the Q vector applied to diagnosing surface frontogenesis and vertical motion. *Mon. Wea. Rev.,* **127,** 2796–2821.

Raymond, D. J., G. B. Raga, C. S. Bretherton, J. Molinari, C. López-Carrillo, and Z. Fuchs, 2003: Convective forcing in the intertropical convergence zone of the eastern Pacific. *J. Atmos. Sci.,* **60,** 2064–2082.

——, C. S. Bretherton, and J. Molinari, 2006: Dynamics of the intertropical convergence zone of the east Pacific. *J. Atmos. Sci.,* **63,** 582–597.

Scott, R. K., J.-P. Cammas, P. Mascart, and C. Stolle, 2001: Stratospheric filamentation into the upper tropical troposphere. *J. Geophys. Res.,* **106,** 11 835–11 848.

Slingo, J. M., 1998: Extratropical forcing of tropical convection in a northern winter simulation with the UGAMP GCM. *Quart. J. Roy. Meteor. Soc.,* **124,** 27–51.

Stein, U., and P. Alpert, 1993: Factor separation in numerical simulations. *J. Atmos. Sci.,* **50,** 2107–2115.

Thorpe, A. J., 1985: Diagnosis of balanced vortex structure using potential vorticity. *J. Atmos. Sci.,* **42,** 397–406.

——, 1997: Attribution and its application to mesoscale structure associated with tropopause folds. *Quart. J. Roy. Meteor. Soc.,* **123,** 2377–2399.

Tomas, R. A., and P. J. Webster, 1994: Horizontal and vertical structure of cross-equatorial wave propagation. *J. Atmos. Sci.,* **51,** 1417–1430.

Waugh, D. W., 2005: Impact of potential vorticity intrusions on subtropical upper tropospheric humidity. *J. Geophys. Res.,* **110,** D11305, doi:10.1029/2004JD005664.

——, and L. M. Polvani, 2000: Climatology of intrusions into the tropical upper troposphere. *Geophys. Res. Lett.,* **27,** 3857–3860.

——, and B. M. Funatsu, 2003: Intrusions into the tropical upper troposphere: Three-dimensional structure and accompanying ozone and OLR distributions. *J. Atmos. Sci.,* **60,** 637–653.

Webster, P. J., and J. R. Holton, 1982: Cross-equatorial response to middle-latitude forcing in a zonally varying basic state. *J. Atmos. Sci.,* **39,** 722–733.